ACS APPLIED MATERIALS & INTERFACES

Research Article

Cite This: ACS Appl. Mater. Interfaces 2019, 11, 16139−16146

www.acsami.org

Formation and Nature of Carbon-Containing Tribofilms

Hongxing Wu,[†,§,#] Arman Mohammad Khan,[†,#] Blake Johnson,[†] Kiran Sasikumar,[∥,⊥] Yip-Wah Chung,*[,†,‡] and Q. Jane Wang*[,†]

[†]Department of Mechanical Engineering and [‡]Department of Materials Science and Engineering, Northwestern University, Evanston, Illinois 60208, United States

[§]Key Laboratory of Education Ministry for Modern Design and Rotor Bearing Systems, Xi'an Jiaotong University, Xi'an 710049, P. R. China

[∥]Avant-Garde Materials Simulation, Deutschland GmbH, Merzhausen 79249, Germany

[⊥]Center for Nanoscale Materials, Argonne National Laboratory, Argonne, Illinois 60439, United States

Supporting Information

ABSTRACT: Minimizing friction and wear at a rubbing interface continues to be a challenge and has resulted in the recent surge toward the use of coatings such as diamond-like carbon (DLC) on machine components. The problem with the coating approach is the limitation of coating wear life. Here, we report a lubrication approach in which lubricious, wear-protective carbon-containing tribofilms can be self-generated and replenishable, without any surface pretreatment. Such carbon-containing films were formed under modest sliding conditions in a lubricant consisting of cyclopropanecarboxylic acid as an additive dissolved in poly-alphaolefin base oil. These tribofilms show the same Raman D and G signatures that have been interpreted to be due to the presence of graphite- or DLC films. Our experimental measurements and reactive molecular dynamics simulations demonstrate that these tribofilms are in fact high-molecular weight hydrocarbons acting as a solid lubricant.

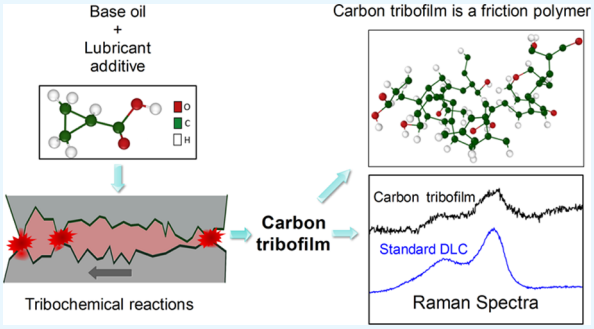

KEYWORDS: *carbon tribofilm, friction polymer, Raman spectroscopy, lubricant additive, DLC film*

1. INTRODUCTION

Carbon-containing films are widely used in engineering systems to reduce friction and wear. In some cases, these films characterized as graphitic or diamond-like carbon (DLC) are deposited by chemical or physical vapor deposition methods, while in others, these films are formed in situ. Publications dated back to as early as 1950s and 1960s[1−3] described the appearance of high molecular weight products formed in sliding metal systems lubricated by hydrocarbons. These products were termed "friction polymers". More recently, Kim et al. noted the formation of polymeric deposits in and around the wear track when the lubrication was provided by vapors of allyl alcohol[4,5] and α-pinene.[6] On the other hand, lubricious carbon films have been reported to form in situ on the bearing surface of cobalt-based metal-on-metal hip implants in an organic medium.[7−10] Some of these films[7−9] were characterized as graphitic from the presence of Raman D and G bands at 1350 and 1580 cm^{-1}, respectively. A lubricious tribofilm was found to form in situ during sliding of nanocomposite MoN−Cu coatings in a polyalphaolefin base oil.[11] Such a film was interpreted to be DLC based on Raman spectroscopy studies as well. Argibay et al.[12] reported the formation of DLC (based on Raman spectroscopy) with a friction coefficient of 0.01 during dry sliding of alumina over the Pt−Au-coated steel surface. This constitutes a rather unique approach for achieving low friction because carbon species were derived from ambient hydrocarbons.

We recently explored the use of cyclopropanecarboxylic acid (CPCa) as a lubricant additive to polyalphaolefin base oil. Because of the metastable nature of the cyclopropane ring, we discovered that this additive dissociates readily during tribological testing under boundary lubrication conditions, resulting in the formation of carbon films, accompanied by reduced friction and wear.[13] The rate of carbon film formation depends on temperature and the contact stress. Raman spectra obtained from these carbon films are similar to those obtained from traditional DLC films synthesized by chemical or physical vapor deposition methods.

The aforementioned findings of in situ formation of carbon films, ascribed to be graphitic, diamond-like, or polymeric, are intriguing because these distinct kinds of carbon films with entirely different structures were produced even though the friction pairs operated under rather modest contact conditions. In comparison, traditional DLC films synthesized by chemical

Received: December 25, 2018
Accepted: April 5, 2019
Published: April 5, 2019

DOI: 10.1021/acsami.8b22496
ACS Appl. Mater. Interfaces 2019, 11, 16139−16146

or physical vapor deposition methods involve nonequilibrium and highly energetic processes. A natural question to ask is how it is possible to obtain graphitic or DLC products using less energetic processes. Another question is whether or not Raman spectroscopy is sufficient for the definitive identification of carbon films as graphitic or DLC. To date, these questions have not been answered, thus hindering the fundamental elucidation of what lubricates the interface in these systems.

Here, the goal is to determine the chemical nature of carbon-containing films formed in situ under typical ball-on-disk tribotesting conditions, using a combination of experimental techniques, viz., Raman, micro-Fourier transform infrared spectroscopy (micro-FTIR), nuclear magnetic resonance (NMR) and mass spectrometry (MS), and reactive molecular dynamics (MD) simulations. Two methods were used to obtain the carbon samples: tribofilms formed during tribotesting in polyalphaolefin (PAO4) containing CPCa and thermal decomposition of CPCa on iron oxide powder surfaces. We will show that these two methods give the same Raman signatures as DLC. The advantage of using the thermal decomposition method to obtain carbon films is its ability to produce sufficiently large quantities of the carbon product for other characterization techniques such as NMR and MS. Reactive MD simulations of CPCa molecules sandwiched between two iron oxide substrates and subjected to tribological conditions were conducted to determine atomic scale processes occurring at surfaces during and after the dissociation of CPCa as well as steps leading to the formation of carbon tribofilms.

2. MATERIALS AND METHODS

2.1. Experimental Details. CPCa (purity of 95%), shown in Figure 1, was obtained from Sigma-Aldrich and used as received.

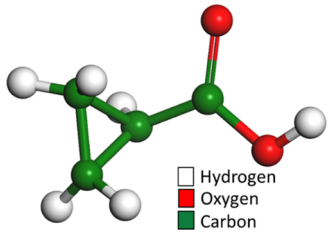

Figure 1. CPCa molecule containing a metastable carbon ring (cyclopropane) and a surface-active group (−COOH) that provides adsorption to the surface.

Fe_3O_4 powders with a particle size of 50−100 nm and a purity of 97% were purchased from Sigma-Aldrich and used as received. The deuterated solvent chloroform-d ($CDCl_3$) was obtained from Cambridge Isotope Laboratories (>99 at. % D) and dried over 0.3 nm molecular sieves. Dichloromethane (DCM) with a purity of 99.8% was obtained from Sigma-Aldrich and used as received. The 1 μm thick DLC film was deposited on a silicon substrate using plasma-enhanced chemical vapor deposition. The gas mixture used in this deposition was 75% hydrogen and 25% methane, producing a DLC film containing 40 atomic % hydrogen. More details of the DLC deposition process were described in a previous paper.[14] PAO4 oil was provided by Valvoline Inc.

A unidirectional ball-on disk tribometer (CETR UMT-2) was used to study the tribological behavior of CPCa.[13] Tribological tests were carried out at a load of 10 N and speed of 0.2 m/s at 25 °C and 24% relative humidity. The ball and disk are AISI 52100 bearing steel with a hardness of about 60 HRC. Disks were polished using standard metallographic techniques to an average surface roughness R_a of 0.06 μm. Steel balls with a diameter of 9.5 mm were obtained from McMaster-Carr. Two lubricant samples were tested: PAO4 (base oil) and PAO4 + 2.5 wt % CPCa. Based on the load, speed, materials used, and test geometry, the average lubricant film thickness/composite root-mean-square surface roughness was computed to be 0.74, indicating that we were operating in the boundary regime. An optical surface profiler (Zygo NewView 7300) was used to image the ball wear scar to determine the wear volume at the end of each test. A dark-colored deposit or tribofilm was observed on the ball at the end of tribotesting with PAO + 2.5 wt % CPCa (see Figure 1). After rinsing with hexane to remove the residual lubricant, we used Raman spectroscopy (HORIBA LabRam HR Evolution Confocal Raman microscope) and micro-FTIR (Bruker LUMOS FTIR Microscope) to study such a deposit. Raman spectroscopy studies were carried out using a laser wavelength of 473 nm with an analyzed area of 10 μm^2. Micro-FTIR measurements were performed with a 32× objective lens and an analyzed area of 50 μm^2. An LEXT OLS 5000 laser confocal microscope was used to obtain the surface topography of surfaces onto which the friction and thermal products were formed.

Carbon materials formed by thermal decomposition of CPCa were obtained by heating a mixture of 0.1 g Fe_3O_4 with 0.3 g CPCa for 3 h at 473 K. The brown residue formed in this process was dissolved in DCM. The resulting solution was filtered and allowed to dry by evaporation under ambient conditions. The residue has a brown color. In addition to Raman spectroscopy, we performed FTIR spectroscopy and proton NMR experiments on this residue. Chemical shifts were referenced using internal solvent resonances. Molecular weight of the thermal product was measured by electrospray ionization (ESI) and matrix-assisted laser desorption/ionization (MALDI) MS, using an Agilent 6210A LCTOF high-resolution time-of-flight mass spectrometer connected to Agilent 1200 series HPLC and a Bruker AutoFlex III MALDI-TOF mass spectrometer with 2,5-dihydroxybenzoic acid as the matrix, respectively.

2.2. Computational Approach. The atomistic simulation model consists of two iron oxide (Fe_3O_4) substrate slabs with CPCa molecules confined within the gap between these two slabs, as shown in Figure 2. Fe_3O_4 was chosen because this is a common oxide phase present on lightly alloyed steel surfaces due to air exposure.[15] The

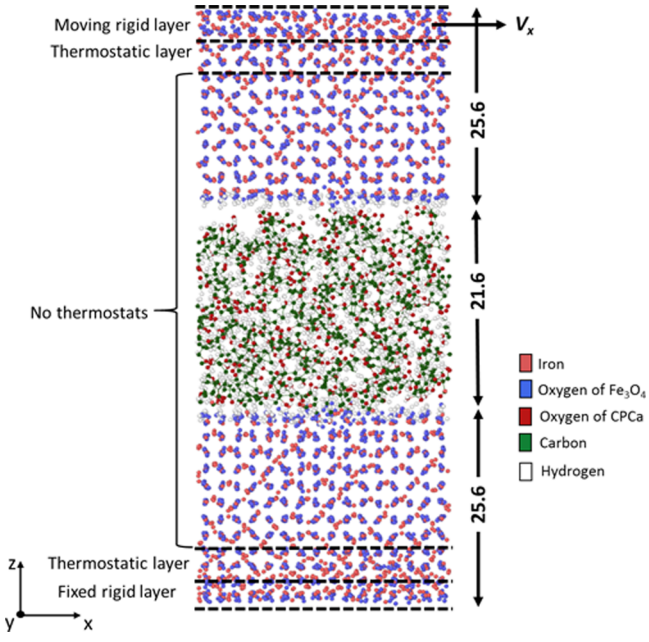

Figure 2. Schematic representation of the computational setup. Dimensions in angstroms of the supercell shown are after equilibrium. The division of the supercell is only done after the equilibration phase, and thermostats applied to different zones are shown.

DOI: 10.1021/acsami.8b22496
ACS Appl. Mater. Interfaces 2019, 11, 16139−16146

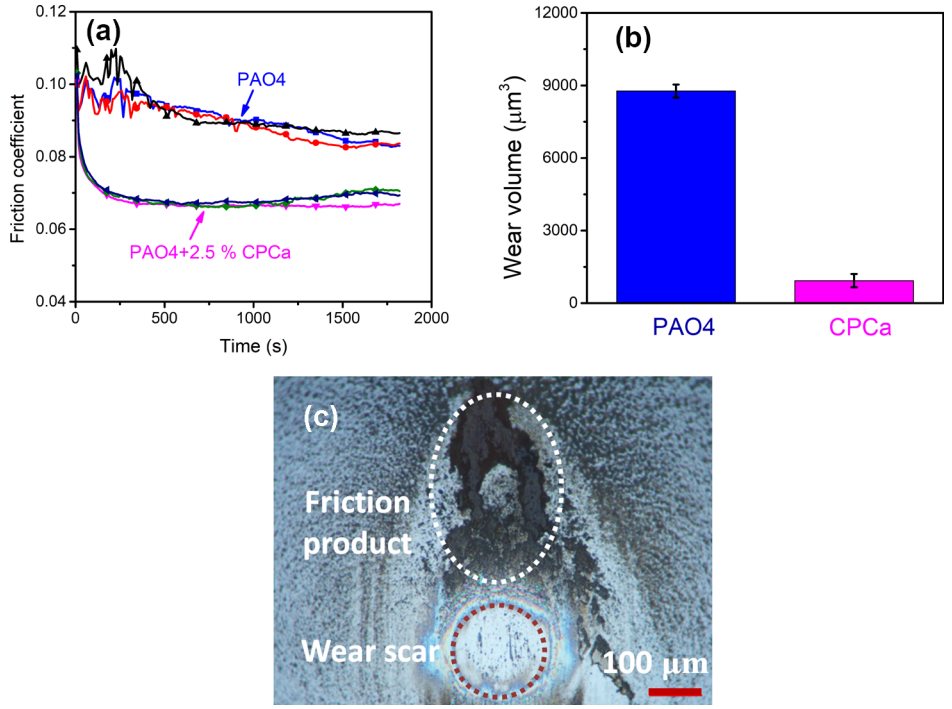

Figure 3. (a) Comparison of friction coefficient vs time under 10 N and 0.2 m/s, using PAO4 and PAO4 + 2.5 wt % CPCa, from three replicates of experiments; (b) comparison of the volume of ball wear after 1800 s tribotesting using PAO4 and PAO4 + 2.5 wt % CPCa; and (c) optical micrograph of the wear scar of a tested ball after tribotesting showing tribofilm formation.

initial dimensions of the setup were 34.13, 34.13, and 73.08 Å in the *x*, *y*, and *z*-directions, respectively. We sandwiched 200 CPCa molecules between the two substrates and applied periodic boundary conditions along the *x*- and *y*-directions. Thickness of each slab in the initial configuration is also shown in Figure 2. Both Fe_3O_4 substrate surfaces were passivated by saturating them with an initial layer of hydrogen atoms.

The simulations were conducted by the large-scale atomic/molecular massively parallel simulator.[16] The reactive force field (ReaxFF) method, a highly transferable force field used for hydrocarbons, was employed in this study. ReaxFF is an empirical force field that uses bond order/bond distance relationships to determine atomic interactions. It can allow a chemical bond to form and break dynamically during the simulation and is thus capable of capturing tribochemical reactions, which is our major objective. The complete details of ReaxFF have been described previously by van Duin et al.[17] Iron oxide parameters used were derived from a recently developed ReaxFF parameters for iron-oxyhydroxide systems.[18]

The simulation was conducted in three stages. First, the initial configuration was allowed to come to equilibrium at 300 K under a pressure of 1 atm (0.1 MPa) for 0.1 ns, long enough for equilibrium to set in. After this stage, the entire simulation domain was divided into three layers along the *z*-direction, as shown in Figure 2. The two outermost layers were defined as fixed rigid layers to keep their structure intact as well as to induce normal and shear loads during the simulation. In the second stage of the simulation, loading along the *z*-direction was conducted for 0.1 ns with temperature and pressure maintained at 300 K and 1 atm, respectively. A normal load F_z, corresponding to 3 GPa, was applied to the topmost rigid layer while keeping the bottom rigid layer fixed. In the third stage, shearing motion was induced by applying a velocity V_x of 10 m/s to the topmost rigid layer while maintaining the normal load applied in the second stage. During sliding, the two adjacent layers, which are below the top rigid layer and above the bottom fixed layer, respectively, were coupled to a thermostat maintained at 473 K. This setup allows dissipation of heat generated due to friction at the sliding interface, with the remaining atoms in the simulation domain free of any constraints, thus allowing them to move and interact freely according to the prescribed interatomic forces. This stage was conducted for 1.8 ns. We used time steps of 0.25 fs throughout the simulation. Molecular visualizations were done by the OVITO software.[19] All quantum mechanical energy calculations were carried out using Gaussian 09.

3. RESULTS AND DISCUSSION

3.1. Tribotesting and Friction-Induced Formation of Carbon Films. Figure 3a shows the evolution of friction coefficient versus time for three separate tests under conditions described in the preceding section, using PAO4 and PAO4 + 2.5 wt % CPCa. Figure 3b compares the total wear sustained by the ball at the end of the test (for a total sliding distance of 360 m). Addition of 2.5 wt % CPCa to PAO4 results in significant reduction in friction and wear. These results are similar to those observed previously.[13] At the end of the tribotesting experiment using PAO4 + 2.5 wt % CPCa, we noted the formation of a dark-colored deposit or tribofilm at the trailing end of the wear scar, as shown in Figure 3c. For ease of reference, we will call this deposit "friction product". To measure the thickness of the friction product, we determined the profile of the trailing edge of the wear scar using laser confocal microscopy, where the tribofilm was observed, before and after dissolving the tribofilm with DCM. Using this procedure, we measured the thickness of the friction product to be 2.6 ± 0.08 μm.

3.2. Synthesis of Carbon Films from Thermal Decomposition of CPCa on Iron Oxide. We held a mixture of 0.1 g Fe_3O_4 powders and 0.3 g of CPCa at 473 K for 3 h in air, after which we observed a brown-colored film coating the Fe_3O_4 powders. Here, Fe_3O_4 was used to model a normal steel surface.[20] We used 473 K for an extended period of time to ensure complete evaporation of CPCa (boiling point of CPCa = 458 K). One may therefore conclude from the appearance of the brown-colored film that a new product has been formed.

DOI: 10.1021/acsami.8b22496
ACS Appl. Mater. Interfaces 2019, 11, 16139−16146

For ease of reference, we will call this "thermal product". Interestingly, the thermal product can be dissolved in DCM, as shown in Figure 4a. After complete evaporation of DCM, the thermal product reappears as a dark brown residue (Figure 4b). The thickness of the thermal product prepared on a silicon wafer was measured to be 0.9 ± 0.2 μm.

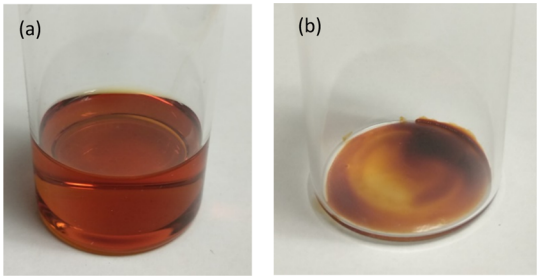

Figure 4. (a) Thermal product dissolved in DCM; and (b) formation of a dark brown residue after drying of (a).

Figure 5a compares the Raman spectra obtained from the friction product and thermal product, as well as DLC obtained by plasma-assisted chemical vapor deposition.[21] Both friction and thermal products show the usual D and G band signature characteristics of DLC. As noted in the Introduction section, we were intrigued by the observation that DLC can be synthesized under these rather modest conditions.

We then compared the thermal stability of these three films by heating them to 623 K for half an hour. Figure 5b shows that the D and G bands of the thermal and friction products almost disappeared completely after heating. In contrast, the D and G bands from the DLC film remain unchanged. This indicates that although the two carbon products show the same DLC Raman signatures, their thermal stability is quite different from DLC, suggesting that the composition of these two carbon products may be different from DLC.

Figure 6 shows the FTIR spectra obtained from the three carbon films. Spectroscopically, the thermal and friction products are almost identical to each other in Figure 6a, and their spectra are quite different from that of the DLC film in Figure 6b. In many ways, both spectra of thermal and friction products are unremarkable: O−H stretch around 3400 cm^{-1}, C−H stretch between 2800 and 3000 cm^{-1}, and CH_2 bending at ∼1450 cm^{-1}. What is most interesting is the absence of strong peaks in the 700 and 900 cm^{-1} range in Figure 6a, which should be present in aromatic compounds due to out-of-plane C−H bending modes. In contrast, the DLC film in Figure 6b reveals strong peaks in this range, suggesting that the friction and thermal products must be different from DLC.

3.3. Characterization of the Thermal Product. Figure 7 shows the proton NMR spectrum obtained from the thermal product dissolved in deuterated trichloromethane ($CDCl_3$). Peaks at 0.89 and 1.24 ppm are due to $-CH_3$ and $-CH_2$ in linear alkyl groups, respectively. There is no signal from CPCa (which would have given peaks at 0.93, 1.05, and 1.59 ppm). The peak at 5.27 ppm is due to the residual DCM solvent. Aromatic compounds should show peaks in the 6−8 ppm range. However, except the peak at 7.24 ppm (reference deuterium signal from $CDCl_3$), no such signal can be observed. Together with the FTIR results shown in Figure 6, we are confident to conclude that the thermal product is *not* an aromatic compound.

Figure 8a shows the mass spectrum obtained from the thermal product using the ESI method, while Figure 8b is the mass spectrum from the same sample using the MALDI method. The observed maximum molecular weight is in excess of 1500, which is much larger than that of CPCa (86). The combined results obtained from FTIR and NMR indicate that the carbon film formed after the exposure of CPCa to iron oxide at 473 K is a high-molecular-weight hydrocarbon or polymer without any graphitic feature, quite different from traditional DLC.

3.4. Comparison of Friction Product, Thermal Product, and DLC. Figure 9 shows two optical images near the ball wear scar after rinsing with hexane and DCM. Note the dark-colored deposit or tribofilm (friction product) near the trailing edge of the wear scar (circled region in Figure 9a) obtained after tribotesting with PAO4 + 2.5 wt % CPCa. Figure 9b shows what happens after rinsing with DCM—note the disappearance of the friction product. This visual evidence indicates that the friction product is soluble in DCM, just like the thermal product.

Figure 10a compares the Raman spectrum of the friction product after rinsing with hexane and DCM. Note the disappearance of the D and G band signatures after rinsing with DCM, consistent with the observation that the friction product is soluble in DCM (Figure 9). Figure 10b compares the Raman spectrum of DLC before and after 20 h immersion in DCM. There is a minor decrease in the D and G band intensities, indicating that traditional DLC is not soluble in DCM, unlike the friction and thermal products.

Based on the experimental characterization of the three different types of carbon films, as shown in Table 1, it is reasonable to conclude that the friction product is essentially

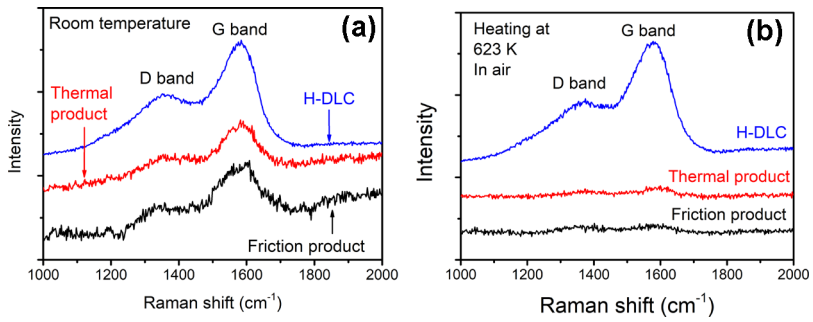

Figure 5. Raman spectra of the friction product, thermal product, and a DLC film (labeled H-DLC). (a) All three carbon materials show characteristic D and G bands at room temperature; (b) after heating at 623 K for 0.5 h, both D and G bands almost disappear for the friction and thermal products but remain unchanged for the DLC film.

DOI: 10.1021/acsami.8b22496
ACS Appl. Mater. Interfaces 2019, 11, 16139−16146

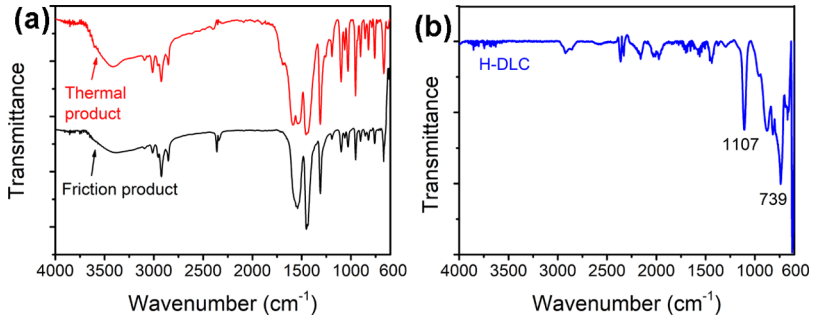

Figure 6. FTIR spectra of three carbon films. (a) Thermal and friction products (micro-reflection mode); and (b) DLC film (ATR mode).

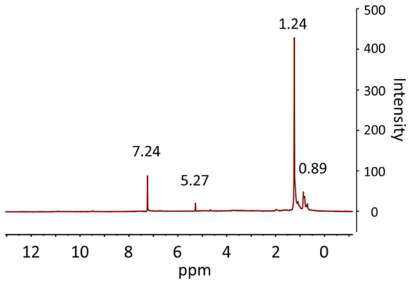

Figure 7. NMR spectrum obtained from the thermal product.

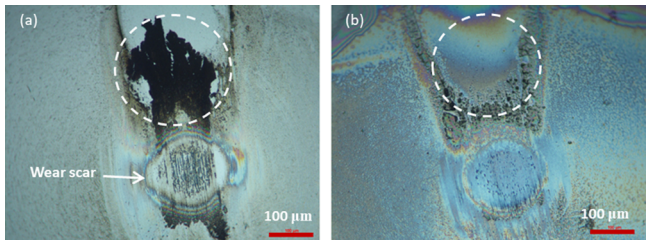

Figure 9. Optical microscope images obtained from near the ball wear scar after tribotesting in PAO4 + 2.5 wt % CPCa: (a) after rinsing with hexane to remove residual lubricant, and (b) after rinsing with DCM.

the same as the thermal product but is different from traditional DLC. Furthermore, based on FTIR, NMR, and MS data, we conclude that the friction and thermal products derived from the dissociation of CPCa on iron oxide are high-molecular weight hydrocarbons, traditionally referred to as friction polymers.

One important lesson learned from this work is the interpretation of the Raman D and G bands in DLC. The D band around 1350 cm^{-1} is assigned to the breathing mode of -sp^2 hybridized atoms in the carbon ring,[22−24] while the G band around 1580 cm^{-1} corresponds to the stretching vibrations of the -sp^2 hybridized C in both chains and rings.[22,24] However, one should note that many hydrocarbons have Raman-active peaks in the vicinity of D and G bands at 1350 and 1580 cm^{-1}. For example, the Raman peak corresponding to $-CH_3$ symmetric bending when the methyl group is attached to C═C or C═O occurs near 1380 cm^{-1};[25] the $=CH_2$ bending and C═C stretching vibrations in adsorbed olefins shift to around 1350[26−28] and 1590 cm^{-1}, respectively.[27,28] Given the likely heterogeneity of these friction polymer molecules, one would expect these peaks to broaden, producing Raman features that look like traditional D and G peaks observed in DLC. The above results demonstrate that *the existence of Raman peaks in the vicinity of 1350 and 1580 cm^{-1} cannot be used as the sole evidence for the formation of traditional DLC.*

3.5. Computational Results. In order to understand these experimental findings and seek more information about the formation of the friction/thermal product, we performed reactive MD simulations, replicating the tribology experimental setup (Figure 2). Our simulations revealed clear evidence of CPCa fragmentation and subsequent polymerization of these fragments. To follow the progress of the carbon film formation, we counted the number of the carbon-containing fragments (C-fragments) during the simulation. We classify C-fragments into three groups according to carbon count per fragment, viz., (A) ≤4, (B) >4 but ≤10, and (C) >10. Figure 11a shows the distributions of carbon atoms within these three groups as a function of time. Before sliding begins, the majority of carbon atoms belong to group A and very few to group B and C, indicating that CPCa remains stable during this time. Note that the molecules in group B before 0.2 ns are dimers formed due to hydrogen bonding between carboxylic groups. Occasional aggregates with carbon count of 12 or 16 with their cyclopropane rings intact form temporarily and then disperse during this equilibration period. As soon as sliding begins, one observes the drop in group A fragment counts, indicating the

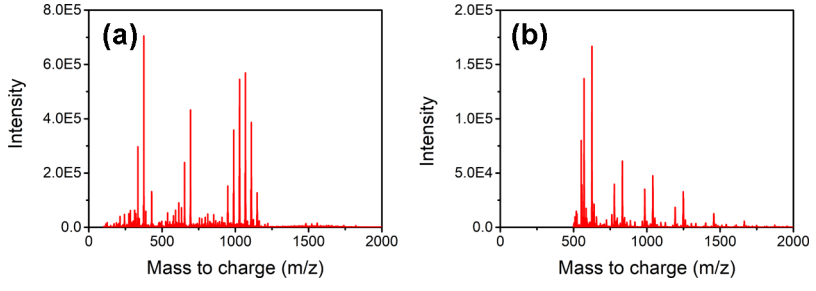

Figure 8. Mass spectra obtained from the thermal product measured by two methods: (a) ESI; and (b) MALDI.

DOI: 10.1021/acsami.8b22496
ACS Appl. Mater. Interfaces 2019, 11, 16139−16146

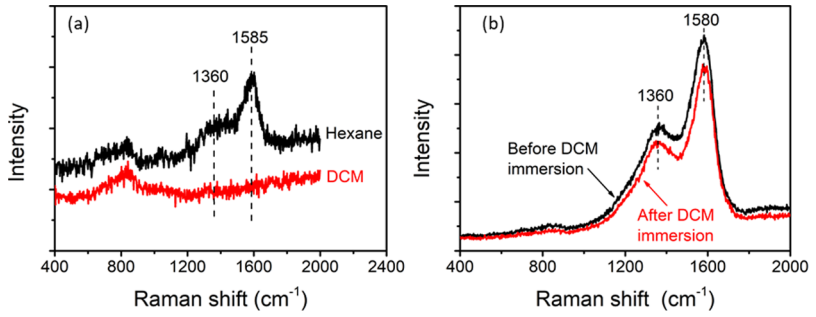

Figure 10. Raman spectra obtained from (a) the friction product after rinsing with hexane and DCM, and (b) DLC before and after immersion for 20 h in DCM.

Table 1. Characterization of Three Different Types of Carbon Films

item	friction product	thermal product	DLC
Raman (D, G band, cm^{-1})	1350, 1580−1600	1350, 1580	1350, 1580
FTIR	identical to each other, not graphitic		graphitic
solubility	soluble in DCM	soluble in DCM	insoluble in DCM
NMR		no aromatics	
MS		>1500 amu	
decomposition temperature (in air)	623 K	623 K	>673 K

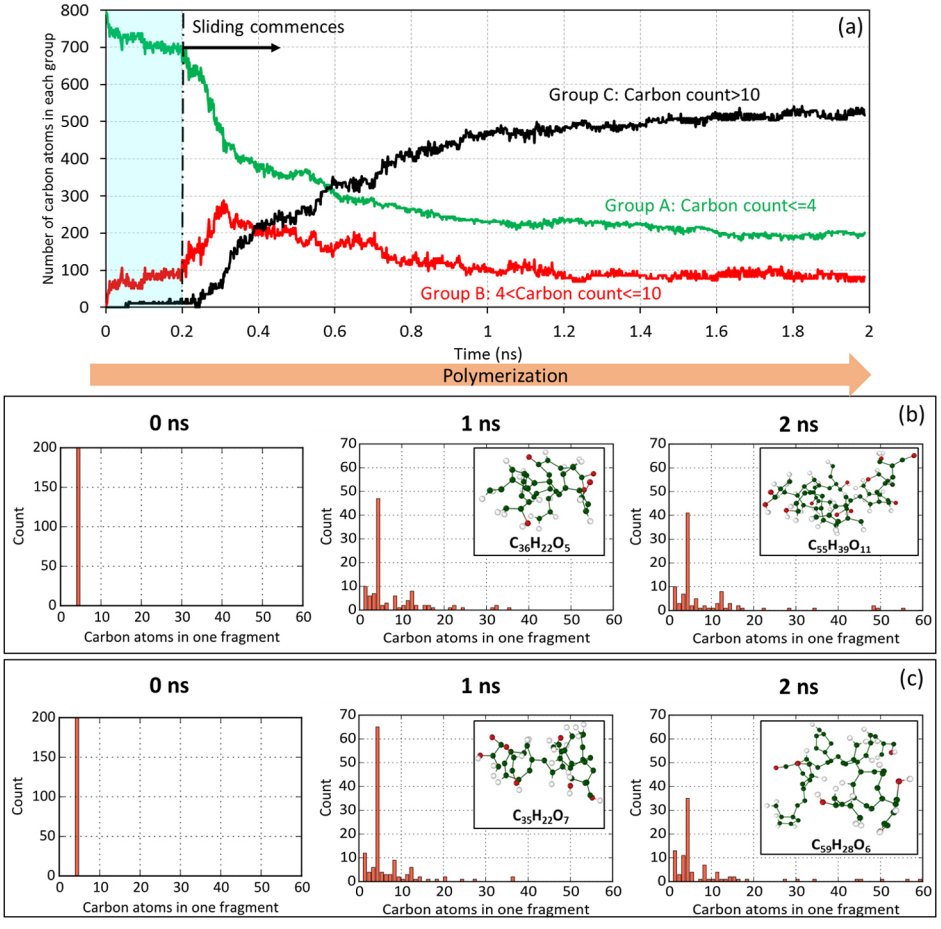

Figure 11. Polymerization of CPCa during the friction process as revealed from MD simulations: (a) time evolution of the number of C-fragments vs their carbon count. Continuous increase in group C suggests a polymerization process; (b) C-fragment distributions of the friction product at selected times are shown, confirming the occurrence of the polymerization process. Note the difference in the *y*-scale for the histogram distributions. The largest fragment at each timestep is also shown in inset; (c) C-fragment distributions of the thermal product at selected times are shown, confirming similar distributions as that of the friction product. Note the difference in the *y*-scale for the histogram distributions. The largest fragment at each timestep is also shown in inset.

DOI: 10.1021/acsami.8b22496
ACS Appl. Mater. Interfaces 2019, 11, 16139−16146

dissociation of CPCa molecules. These broken smaller fragments then start to recombine, resulting in the surge of group B fragments between 0.2 and 0.4 ns and the build-up of large group C fragments. By 2 ns, 520 out of 800 total carbon atoms in the simulation system are in group C, suggesting the tendency to form polymers.

To further convince ourselves about the similar nature of the thermal and friction products formed in our experiments, we conducted MD simulations to produce the thermal product and compared it with the friction product. Frictional heating under tribological conditions used in the simulations increases the interfacial temperature from 300 to about 730 K (Figure S6). We explored the polymerization process with the same initial configuration, temperature profile, and load as those in the friction process but no sliding. Figure 11b,c shows similar histogram distributions of the carbon fragments produced by the friction and thermal processes as obtained from MD simulations, demonstrating the buildup of higher molecular weight hydrocarbons[29] (data for more intermediate steps for the friction product being provided in Figure S5). By the end of the simulation, fragments with 48, 49, and 55 carbon atoms are formed in the frictional process and 50, 55, and 59 in the thermal process. At the end of the 2 ns simulation, the molecular weight of the largest fragment is 832 for the friction product and 874 for the thermal product, about a factor of two less than that observed by MS (Figure 8). There are two possible reasons for this mismatch. First, there is a large difference in the time scales involved. Second, there may be limited availability of reactant molecules in the simulation study, in which we used only 200 CPCa molecules, containing 800 carbon atoms. Generation of the three largest fragments consumes more than 20% of the initial CPCa molecules. Given these limitations of MD simulation, we consider the moderate mismatch between experiment and simulation to be not too surprising.

Our previous study[13] indicates that contact stress has two effects. One is temperature because of flash heating as shown by MD simulation above. The other is the activation energy for tribofilm formation. The zero-stress activation energy was found to be almost identical to C−C bond scission in cyclopropane. This suggests that (1) the rate-limiting step in tribofilm formation is the fragmentation of CPCa, and (2) that the contact stress influences CPCa fragmentation. One mechanism for the latter suggested by Tysoe is the contact stress affecting the position and orientation of adsorbed molecules involved in the tribochemical reaction.[30] Another mechanism hypothesized by Yeon et al.[4] is molecular deformation induced by the contact stress. Both mechanisms are possible, given the metastable nature of CPCa molecules used in our experiments.

4. CONCLUSIONS

This paper presents the results of a study exploring the formation and chemical nature of carbon-containing tribofilms. These carbon films were generated by two methods: tribotesting using PAO base oil containing 2.5 wt % CPCa as the additive (friction product) and thermal decomposition of CPCa on iron oxide powders (thermal product). Both friction and thermal products show the same D and G peak characteristics of DLC but both products decompose at 623 K in air, while DLC remains stable at >673 K. Moreover, friction and thermal products are soluble in DCM and have almost identical FTIR spectra, in stark contrast to DLC (insoluble in DCM and very different FTIR spectrum). Together with MS studies, we conclude that the friction and thermal products are not traditional DLC but are high-molecular weight hydrocarbons. A corollary to this study is that the presence of Raman D and G bands should not be used as the sole evidence for the formation of graphitic or DLC.

■ ASSOCIATED CONTENT

Supporting Information

The Supporting Information is available free of charge on the ACS Publications website at DOI: 10.1021/acsami.8b22496.

Thermal behavior of friction and thermal products, MD simulation, including validation of the ReaxFF method, atomic mechanisms, and analysis of reaction products along with bond order information used (PDF)

■ AUTHOR INFORMATION

Corresponding Authors

*E-mail: ywchung@northwestern.edu (Y.-W.C.).
*E-mail: qwang@northwestern.edu (Q.J.W.).

ORCID

Hongxing Wu: 0000-0002-0304-0740

Author Contributions

#H.W. and A.M.K. contributed equally to this work.

Notes

The authors declare no competing financial interest.

■ ACKNOWLEDGMENTS

The authors would like to thank the support from the US National Science Foundation (grant no. CMMI-1662606) and Northwestern University (the McCormick Research Catalyst Awards Fund grant no. 10038293). We thank Valvoline for providing PAO lubricants, Dr. Ali Erdemir for providing the DLC film, and Profs. Jiaxing Huang, Hong Liang, and Ashlie Martini for critical reading of this manuscript. This work made use of the Keck-II Facility of Northwestern University's NUANCE Center, which has received support from the Keck Foundation, the Soft and Hybrid Nanotechnology Experimental (SHyNE) Resource (NSF ECCS-1542205), the Materials Research Center (NSF DMR-1121262), the McCormick Research Catalyst Awards Fund, grant no. 10038293, and the International Institute for Nanotechnology (IIN) at Northwestern University. We would like to thank Dr. Xinqi Chen for his help in conducting FTIR spectroscopy. Helpful discussions with Professor Guangneng Dong in Xi'an Jiaotong University, Dr. Xingliang He and Dr. Michael Desanker are acknowledged. H.W. would also like to acknowledge the scholarship support from China Scholarship Council (CSC, no. 201606280181). This research was supported in part through the computational resources and staff contributions provided for the Quest high performance computing facility at Northwestern University, which is jointly supported by the Office of the Provost, the Office for Research, and Northwestern University Information Technology. The research also used computational resources from Center of Nanoscale Materials (CNM) as result of accepted user proposal number CNM 56595. Use of the Center for Nanoscale Materials, an Office of Science user facility, was supported by the U.S. Department of Energy, Office of Science, Office of Basic Energy Sciences, under contract no. DE-AC02-06CH11357.

DOI: 10.1021/acsami.8b22496
ACS Appl. Mater. Interfaces 2019, 11, 16139−16146

REFERENCES

(1) Hermance, H. W.; Egan, T. F. Organic Deposits on Precious Metal Contacts. *Bell Labs Tech. J.* **1958**, *37*, 739−776.
(2) Fein, R. S.; Kreuz, K. L. Chemistry of Boundary Lubrication of Steel by Hydrocarbons. *ASLE Trans.* **1965**, *8*, 29−38.
(3) Klaus, E. E.; Duda, J. L.; Chao, K. K. A Study of Wear Chemistry Using a Micro Sample Four-Ball Wear Test. *Tribol. Trans.* **1991**, *34*, 426−432.
(4) Yeon, J.; He, X.; Martini, A.; Kim, S. H. Mechanochemistry at Solid Surfaces: Polymerization of Adsorbed Molecules by Mechanical Shear at Tribological Interfaces. *ACS Appl. Mater. Interfaces* **2017**, *9*, 3142−3148.
(5) He, X.; Barthel, A. J.; Kim, S. H. Tribochemical synthesis of nano-lubricant films from adsorbed molecules at sliding solid interface: Tribo-polymers from α-pinene, pinane, and n-decane. *Surf. Sci.* **2016**, *648*, 352−359.
(6) He, X.; Kim, S. H. Mechanochemistry of Physisorbed Molecules at Tribological Interfaces: Molecular Structure Dependence of Tribochemical Polymerization. *Langmuir* **2017**, *33*, 2717−2724.
(7) Liao, Y.; Pourzal, R.; Wimmer, M. A.; Jacobs, J. J.; Fischer, A.; Marks, L. D. Graphitic Tribological Layers in Metal-on-Metal Hip Replacements. *Science* **2011**, *334*, 1687−1690.
(8) Wimmer, M. A.; Laurent, M. P.; Mathew, M. T.; Nagelli, C.; Liao, Y.; Marks, L. D.; Jacobs, J. J.; Fischer, A. The Effect of Contact Load on CoCrMo Wear and the Formation and Retention of Tribofilms. *Wear* **2015**, *332*−*333*, 643−649.
(9) Wimmer, M. A.; Fischer, A.; Büscher, R.; Pourzal, R.; Sprecher, C.; Hauert, R.; Jacobs, J. J. Wear Mechanisms in Metal-on-Metal Bearings: The Importance of Tribochemical Reaction Layers. *J. Orthop. Res.* **2010**, *28*, 436−443.
(10) Hesketh, J.; Ward, M.; Dowson, D.; Neville, A. The Composition of Tribofilms Produced on Metal-on-Metal Hip Bearings. *Biomaterials* **2014**, *35*, 2113−2119.
(11) Erdemir, A.; Ramirez, G.; Eryilmaz, O. L.; Narayanan, B.; Liao, Y.; Kamath, G.; Sankaranarayanan, S. K. R. S. Carbon-based Tribofilms from Lubricating Oils. *Nature* **2016**, *536*, 67−71.
(12) Argibay, N.; Babuska, T. F.; Curry, J. F.; Dugger, M. T.; Lu, P.; Adams, D. P.; Nation, B. L.; Doyle, B. L.; Pham, M.; Pimentel, A.; Mowry, C.; Hinkle, A. R.; Chandross, M. In-situ tribochemical formation of self-lubricating diamond-like carbon films. *Carbon* **2018**, *138*, 61−68.
(13) Johnson, B.; Wu, H.; Desanker, M.; Pickens, D.; Chung, Y.-W.; Wang, Q. J. Direct Formation of Lubricious and Wear-Protective Carbon Films from Phosphorus-and Sulfur-Free Oil-Soluble Additives. *Tribol. Lett.* **2018**, *66*, 2.
(14) Erdemir, A. The role of hydrogen in Tribological Properties of Diamond-Like Carbon Films. *Surf. Coat. Technol.* **2001**, *146*−*147*, 292−297.
(15) Fursey, A. Oxide Films on Mild Steel. *Nature* **1965**, *207*, 747.
(16) Plimpton, S. Fast Parallel Algorithms for Short-Range Molecular Dynamics. *J. Comput. Phys.* **1995**, *117*, 1−19.
(17) van Duin, A. C. T.; Dasgupta, S.; Lorant, F.; Goddard, W. A. ReaxFF: A Reactive Force Field for Hydrocarbons. *J. Phys. Chem. A* **2001**, *105*, 9396−9409.
(18) Aryanpour, M.; van Duin, A. C. T.; Kubicki, J. D. Development of a Reactive Force Field for Iron−Oxyhydroxide Systems. *J. Phys. Chem. A* **2010**, *114*, 6298−6307.
(19) Stukowski, A. Visualization and Analysis of Atomistic Simulation Data with OVITO−the Open Visualization Tool. *Modell. Simul. Mater. Sci. Eng.* **2010**, *18*, 015012.
(20) Grosvenor, A. P.; Kobe, B. A.; McIntyre, N. S. Studies of the oxidation of iron by water vapour using X-ray photoelectron spectroscopy and QUASES. *Surf. Sci.* **2004**, *572*, 217−227.
(21) Erdemir, A.; Eryilmaz, O. L.; Fenske, G. Synthesis of Diamondlike Carbon Films with Superlow Friction and Wear Properties. *J. Vac. Sci. Technol., A* **2000**, *18*, 1987−1992.
(22) Ferrari, A. C.; Robertson, J. Raman spectroscopy of amorphous, nanostructured, diamond-like carbon, and nanodiamond. *Philos. Trans. R. Soc., A* **2004**, *362*, 2477−2512.
(23) Chu, P. K.; Li, L. Characterization of Amorphous and Nanocrystalline Carbon Films. *Mater. Chem. Phys.* **2006**, *96*, 253−277.
(24) Ferrari, A.; Robertson, J. Resonant Raman Spectroscopy of Disordered, Amorphous, and Diamondlike Carbon. *Phys. Rev. B: Condens. Matter Mater. Phys.* **2001**, *64*, 075414.
(25) Lin-Vien, D.; Colthup, N. B.; Fateley, W. G.; Grasselli, J. G. *The Handbook of Infrared and Raman Characteristic Frequencies of Organic Molecules*; Elsevier, 1991.
(26) Moskovits, M.; Dilellla, D. P. Enhanced Raman Spectra of Ethylene and Propylene Adsorbed on Silver. *Chem. Phys. Lett.* **1980**, *73*, 500−505.
(27) Akemann, W.; Otto, A. Vibrational Frequencies of C_2H_4 and C_2H_6 Adsorbed on Potassium, Indium, and Noble Metal Films. *Langmuir* **1995**, *11*, 1196−1200.
(28) Gammage, M. D.; Stauffer, S.; Henkelman, G.; Becker, M. F.; Keto, J. W.; Kovar, D. Ethylene Binding to Au/Cu Alloy Nanoparticles. *Surf. Sci.* **2016**, *653*, 66−70.
(29) Khajeh, A.; He, X.; Yeon, J.; Kim, S. H.; Martini, A. Mechanochemical Association Reaction of Interfacial Molecules Driven by Shear. *Langmuir* **2018**, *34*, 5971−5977.
(30) Tysoe, W. On Stress-Induced Tribochemical Reaction Rates. *Tribol. Lett.* **2017**, *65*, 48.

DOI: 10.1021/acsami.8b22496
ACS Appl. Mater. Interfaces 2019, 11, 16139−16146